



HAL
open science

Statistics of the Stokes parameters for the signal scattered by layered structures with an arbitrary number of slightly rough interfaces

Richard Dusséaux, Saddek Afifi

► **To cite this version:**

Richard Dusséaux, Saddek Afifi. Statistics of the Stokes parameters for the signal scattered by layered structures with an arbitrary number of slightly rough interfaces. *IEEE Transactions on Geoscience and Remote Sensing*, 2022, 60, pp.Art no. 2006912. 10.1109/TGRS.2022.3209814 . insu-03793376

HAL Id: insu-03793376

<https://insu.hal.science/insu-03793376>

Submitted on 3 Oct 2022

HAL is a multi-disciplinary open access archive for the deposit and dissemination of scientific research documents, whether they are published or not. The documents may come from teaching and research institutions in France or abroad, or from public or private research centers.

L'archive ouverte pluridisciplinaire **HAL**, est destinée au dépôt et à la diffusion de documents scientifiques de niveau recherche, publiés ou non, émanant des établissements d'enseignement et de recherche français ou étrangers, des laboratoires publics ou privés.

Statistics of the Stokes Parameters for the Signal Scattered by Layered Structures with an Arbitrary Number of Slightly Rough Interfaces.

Richard Dusséaux and Saddek Afifi

Richard Dusséaux is with the Laboratoire Atmosphères, Milieux, Observations Spatiales (LATMOS), Université de Versailles Saint-Quentin-en-Yvelines (UVSQ/Paris-Saclay), 11 boulevard d'Alembert, 78280 Guyancourt, France (e-mail: richard.dusseaux@latmos.ipsl.fr).

Saddek Afifi is with the Electronics Department, Badji Mokhtar – Annaba University, BP 12, 23000, Annaba, Algeria (e-mail: saddekafifi@yahoo.fr).

Abstract - Horizontally stratified structures are commonly used to represent naturally occurring structures, such as soils. The electromagnetic signature of such a medium illuminated by a radar and the polarization state of the scattered wave are fully determined by the knowledge of the four Stokes parameters. In this paper, we determine the statistics of the four Stokes parameters for the signal scattered by layered structures with an arbitrary number of slightly rough interfaces. The rough interfaces are realizations of second-order stationary centered Gaussian stochastic processes and the layered structure is illuminated by an elliptically polarized monochromatic wave. The zenithal and azimuthal components of the far scattered electric field are derived from the first-order small perturbation method. The derivation leads to a multivariate Gaussian model for the underlying complex scattered amplitudes and we establish the closed-form expressions of the probability density function, the cumulative density function and the first- and second-order moments for the four Stokes parameters. For an observation direction outside the incidence plane, we establish the condition on the incidence wave parameters for which the zenithal and azimuthal components are uncorrelated. For an air / snow cover / frozen soil / unfrozen soil structure, we analyze the marginal probabilities and validate the theory by comparison with Monte-Carlo simulations. More generally, when the two complex components of the field scattered by the illuminated zone are Gaussian random variables, these statistics offer possibilities for in-depth investigating the polarization of scattering processes from random media.

Index Terms - Layered rough surfaces, scattered field, small perturbation method, Stokes parameters, statistics.

I. INTRODUCTION

Scattering of electromagnetic waves from layered structures has aroused the interest of physicists and engineers for many years with applications in several fields as remote sensing, civil engineering, geophysics and optics. In the field of the remote sensing, multilayered structures with randomly rough boundaries are relevant for modeling the electromagnetic wave scattering signal from natural scenes, such as, stratified soils [1]-[2], snow cover blanket [3]-[4], snow cover ice [5]-[6] or oil slick on sea surface [7]-[8]. A number of numerical and analytical models have been proposed to simulate the response of stratified structures [9]-[11]. The analytical models cannot be compared in terms of computing cost with the exact ones that are associated with numerical techniques and Monte-Carlo simulations. Within their domains of validity, the analytical models allow a fast analysis of the multilayered structures by means of analytical formulae. The small perturbation method (SPM) is often used for the analysis of these scattering phenomena. This method is based on Taylor series of the complex amplitudes of the scattered field and on Taylor series of the boundary value problem and gives analytical formulae for the coherent and incoherent scattered intensities [12]-[18]. The first-order SPM is valid for small height variations compared to the EM wavelength and small gradients of the surface heights compared to 1 [19]-[20]. The second-order SPM solution is significant to characterize the cross-polarized backscattering [15]-[18].

In [12]-[20], the scattered field is characterized by the scattered intensity, i.e. by its second order moment which is already included in the probability distribution of the scattered field. For stratified structure with randomly rough boundaries under electromagnetic wave illumination, the scattered field in a given observation direction is a random variable and the knowledge of the probability density function (PDF) is of great importance for the characterization of the structure. In [21], we established the probability distributions for the modulus, the phase and the intensity of the wave scattered by a stratified medium illuminated by a horizontally (h) or vertically (v) polarized monochromatic plane wave. The interfaces were characterized by Gaussian height distributions with zero mean values. For slightly rough interfaces with a finite extension, we showed that the modulus for the co- and cross-polarized scattering amplitudes follows a Hoyt law and that the phase is not uniformly distributed. For

interfaces with infinite surface area, the modulus follows a Rayleigh law and the phase is uniformly distributed. Within the framework of the first-order SPM, we determined in [22] the PDF of the co-polarized phase difference for the field scattered by a multilayered medium. In [23], we showed that, outside the incidence plane, the cross-polarized phase difference is not uniformly distributed and contains information about the stratified structure. In [24], we derive the closed-form expression of the probability distribution for the scattered intensity ratio and we showed that the co- and cross-polarized intensity ratios follow heavy-tailed distributions. In [25], we showed, still within the framework of the first-order SPM, that the statistics of the co- and cross-polarized intensity ratios allow to differentiate an air/clayey soil/rock structure with or without snow cover.

To reduce statistical variations, polarimetric radars use the multilook processing by averaging spatially the randomly scattered signals. In [26]-[29], the statistics of multilook signatures have been investigated under the assumption of multivariate Gaussian for the understudying scattered amplitudes. In [30], within the framework of SPM, assuming that the n -look intensities are means of n independent identically distributed single look intensities, we derived the statistics for the multilook intensity ratio for a multilayered structure bounded by randomly rough surfaces under a h- or v-polarized plane wave illumination. We obtained a three-parameter probability distribution and we showed that the PDF only depends on the number of looks, on the modulus of the complex correlation coefficient between the scattered amplitudes under study, and on the ratio between the associated average single-look intensities. In [31], the work was extended to the distribution of the phase difference between two multilook scattered signals. We showed that the phase difference PDF is expressed in terms of the Gauss hypergeometric functions and only depends on the number of looks and on the modulus and phase of the complex correlation coefficient between the scattered amplitudes under study [28].

The description of the scattering signal from layered structures can be obtained using the Stokes parameters. The Stokes parameters are a set of values that describe the polarization state of the scattered field and depend on two orthogonal complex components of the scattered electric field. Statistics of the Stokes parameters depends on the normalized complex correlation coefficient between the two orthogonal components, the modulus and phase of which define the degree of coherence and the mean effective phase difference [32]-[34]. In [32], the obtained statistics were limited to the case where the

mean effective phase difference is equal to 0. In [33], the PDF for the four Stokes parameters was established but for two of the four parameters, the probability law was not given by an analytical expression but in the form of an integral which needed to be numerically evaluated. In [34], the analytical expression for each of the four Stokes parameters was obtained. In [32]-[34], the statistics of the Stokes parameters were investigated under the hypothesis of multivariate Gaussian models for the two underlying orthogonal complex components. The results established in [32]-[34] are still relevant, but the link with an electromagnetic model was not made. For physicists, it is important to derive the probability laws either from an exact electromagnetic model combined with Monte-Carlo simulations [35] or from an analytical approach [36]. Moreover, the results in [32]-[34] did not relate specifically to the scattering of electromagnetic waves by multilayered structures.

In the present study, we focus on the statistical properties of the four Stokes parameters for the single-look signal scattered by layered structures with an arbitrary number of rough interfaces. Compared to our previous works, we are therefore interested in the polarization state of the scattered electric field. We assume that the rough interfaces are realizations of second-order stationary centred Gaussian stochastic processes and that the layered structure is illuminated by an elliptically polarized monochromatic wave. The zenithal and azimuthal components of the far scattered electric field are derived from the first-order SPM. For a stack of homogeneous layers with randomly rough surfaces, the two components of the scattered field depend on rough interface realizations and for a given direction, they are complex random variables. The derivation leads to a multivariate Gaussian model for the underlying complex scattered amplitudes. The values of the Stokes parameters change from one realization of the multilayer structure to another. For a given direction, they are also random variables. By using the multivariate Gaussian model for the zenithal and azimuthal complex components, we establish the closed-form expressions of the probability density function, the cumulative density function (CDF) and the first- and second-order moments for the four Stokes parameters.

This article is organized as follows. Section II reports the statistical properties of the considered three-dimensional stratified structure and the first-order SPM scattering model applied to an elliptically-polarized incident plane wave. For infinite slightly rough surfaces described by Gaussian centered stochastic processes, we show that the real and imaginary parts of the zenithal and azimuthal components

follow a Gaussian joint distribution and we also derive the analytical expression for the degree of coherence and the mean effective phase difference. In Section III, for each of the Stokes parameters, we establish closed-form expressions for the PDF and CDF and for the first- and second-order moments. In section IV, for air/snow cover/frozen soil/unfrozen soil structures, we study the statistics of the Stokes parameters and we validate the theoretical formulae by comparison with Monte-Carlo simulations.

II. PROBLEM FORMULATION

A. Statistics of randomly rough interfaces

As shown in Fig. 1, the structure we consider is a stack of $N - 1$ rough two-dimensional interfaces. For the study, the length L along Ox and Oy axes tends to infinity. For $i \in [1, N - 1]$, the i -th and the $(i + 1)$ -th interfaces are separated by a non-magnetic, homogeneous and isotropic layer with a thickness $d_i = u_{i+1} - u_i$ (with $u_1 = 0$). The i -th layer is characterized by a relative permittivity ϵ_{ri} . The top region (medium 1) is assumed to be air (assimilated to vacuum). The bottom region (medium N) is a half-space. Rough boundaries are realizations of second order stationary, uncorrelated, centered Gaussian stochastic processes with isotropic Gaussian spectrum $\hat{R}_i(\alpha, \beta)$:

$$\hat{R}_i(\alpha, \beta) = \sigma_i^2 l_i^2 \pi \exp\left(-\frac{\alpha^2 + \beta^2}{4} l_i^2\right). \quad (1)$$

Throughout the paper, a function symbol with a superscript ‘^’ stands for the Fourier transform of the function. The quantities α and β are the wave numbers resulting from the 2D Fourier transform of the Gaussian autocorrelation function $R_i(x, y)$ characterizing the i -th interface. The quantity σ_i is the rms-height and l_i , the correlation length.

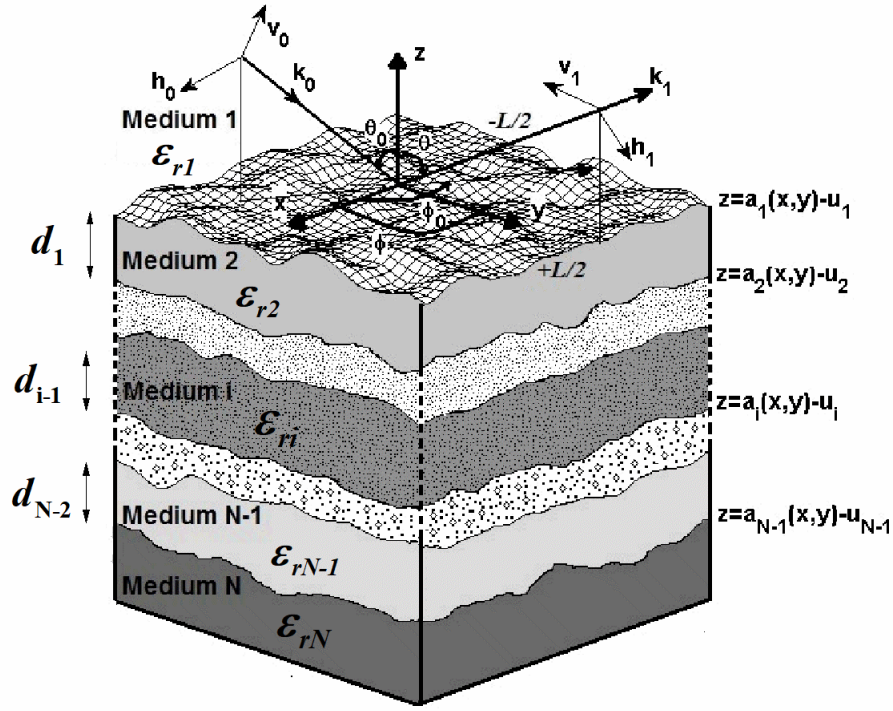


Fig. 1. Structure with an arbitrary number of rough two-dimensional interfaces

Function $a_i(x, y)$ is a realization of an isotropic Gaussian random process with the rms-height σ_i and the correlation length l_i .

B. Polarization and Stokes parameters

Suppose that a horizontally (h) or vertically (v) polarized monochromatic plane wave illuminates the structure. The components $(\alpha_0, \beta_0, -\gamma_0)$ of the incident wave vector \mathbf{k}_0 are defined from the zenith angle θ_0 and the azimuth angle ϕ_0 with $\alpha_0 = k_1 \sin \theta_0 \cos \phi_0$, $\beta_0 = k_1 \sin \theta_0 \sin \phi_0$ and $\gamma_0 = k_1 \cos \theta_0$. The quantity k_1 designates the vacuum wave number. The incident electric field is expressed as follows:

$$\mathbf{E}_0 = (A_{0(h)} \mathbf{h}_0 + A_{0(v)} \mathbf{v}_0) \exp(-j\mathbf{k}_0 \cdot \mathbf{r}). \quad (2)$$

Note that in (2), the time dependence $\exp(+j\omega t)$ (where ω is the pulsation) is dropped. The vector $\mathbf{r}(x, y, z)$ is the position vector in the Cartesian coordinate system. The vectors \mathbf{h}_0 and \mathbf{v}_0 are the incident polarization vectors. For a h-polarized incident plane wave, $A_{0(h)} = 1$ and $A_{0(v)} = 0$. For a v-polarized incident wave, $A_{0(h)} = 0$ and $A_{0(v)} = 1$. The (h)-polarized and (v)-polarized components of the

scattered electric field in the upper half-space are represented by continuous spectra of upward propagating plane waves [21]:

$$\begin{aligned}\mathbf{E}_1^{(ha)}(x, y, z) &= \frac{1}{4\pi^2} \int_{-\infty}^{+\infty} \int_{-\infty}^{+\infty} A_{1(ha)}(\alpha, \beta) \mathbf{h}(\alpha, \beta) \exp(-j\mathbf{k}_1(\alpha, \beta) \cdot \mathbf{r}) d\alpha d\beta \\ \mathbf{E}_1^{(va)}(x, y, z) &= \frac{1}{4\pi^2} \int_{-\infty}^{+\infty} \int_{-\infty}^{+\infty} A_{1(va)}(\alpha, \beta) \mathbf{v}_1(\alpha, \beta) \exp(-j\mathbf{k}_1(\alpha, \beta) \cdot \mathbf{r}) d\alpha d\beta\end{aligned}\quad (3)$$

The letter (a) designates the (h) or (v) incident polarization. The wave vector \mathbf{k}_1 of the elementary plane wave characterized by the wave function $\exp(-j\mathbf{k}_1(\alpha, \beta) \cdot \mathbf{r})$ is defined by

$$\mathbf{k}_1 = \alpha \mathbf{u}_x + \beta \mathbf{u}_y + \gamma_1 \mathbf{u}_z \quad (4)$$

with $\mathbf{k}_1 \cdot \mathbf{k}_1 = k_1^2$ and $\text{Im}(\gamma_1) \leq 0$. The polarization vectors \mathbf{v}_1 and \mathbf{h} and the wave vector \mathbf{k}_1 form a direct trihedron,

$$\begin{aligned}\mathbf{h} &= \frac{\beta \mathbf{u}_x - \alpha \mathbf{u}_y}{\sqrt{\alpha^2 + \beta^2}} \\ \mathbf{v}_1 &= \mathbf{h} \wedge \frac{\mathbf{k}_1}{k_1} = \frac{-\gamma_1(\alpha \mathbf{u}_x + \beta \mathbf{u}_y)}{k_1 \sqrt{\alpha^2 + \beta^2}} + \frac{\sqrt{\alpha^2 + \beta^2}}{k_1} \mathbf{u}_z.\end{aligned}\quad (5)$$

The symbol \wedge designates the vector product. $(\mathbf{u}_x, \mathbf{u}_y, \mathbf{u}_z)$ are the unit vectors in the Cartesian coordinate system. The vectors \mathbf{h}_0 and \mathbf{v}_0 are obtained from (5) replacing $(\alpha, \beta, \gamma_1)$ by $(\alpha_0, \beta_0, -\gamma_0)$. Using the stationary phase method [37]-[38], at the observation point (r, θ, ϕ) located in the far-field zone, we obtain from (3) the horizontal and vertical components of the asymptotic scattered electric field,

$$\begin{aligned}\mathbf{E}_{far}^{(ha)}(r, \theta, \phi) &= -jA_{1(ha)}(\alpha, \beta) \cos \theta \frac{\exp(-jkr)}{\lambda r} \mathbf{u}_\phi \\ \mathbf{E}_{far}^{(va)}(r, \theta, \phi) &= -jA_{1(va)}(\alpha, \beta) \cos \theta \frac{\exp(-jkr)}{\lambda r} \mathbf{u}_\theta\end{aligned}\quad (6)$$

where $\alpha = k_1 \sin \theta \cos \phi$ and $\beta = k_1 \sin \theta \sin \phi$. $(\mathbf{u}_r, \mathbf{u}_\theta, \mathbf{u}_\phi)$ are the unit vectors of the spherical coordinate system.

The polarization of the incident wave is deduced from the complex amplitudes $A_{0(h)}$ and $A_{0(v)}$ with $A_{0(h,v)} = |A_{0(h,v)}| \exp(j\delta_{o(h,v)})$ where $|A_{0(h,v)}|$ designates the modulus of $A_{0(h,v)}$. We note $\delta_{vh} = \delta_{o(v)} - \delta_{o(h)}$ the phase difference. In general, the incident wave is elliptically polarized. If $\delta_{vh} = q\pi$ where q is an

integer or if $|A_{o(h)}|=0$ or $|A_{o(v)}|=0$, the polarization is linear. If $\delta_{vh} = +\pi/2$ and $|A_{o(h)}|=|A_{o(v)}|$, the incident wave is right-handed circularly polarized and the rotation of the electric field and the direction of the wave propagation form a right-handed screw [39]. If $\delta_{vh} = -\pi/2$ and $|A_{o(h)}|=|A_{o(v)}|$, we obtain the left-handed polarization case.

We express the modulus of the complex amplitudes as follows,

$$|A_{0(h,v)}| = \frac{a_{0(h,v)}}{L} \quad (7)$$

in order to obtain an incident power P_0 independent on the $L \times L$ surface area:

$$P_0 = \frac{a_{0(h)}^2 + a_{0(v)}^2}{2Z_1} \cos \theta_0. \quad (8)$$

For an elliptically polarized incident wave, the direction of the scattered electric field vector in the far-field zone is defined by the vector \mathbf{p} ,

$$\mathbf{p} = A_{1\theta} \mathbf{u}_\theta + A_{1\phi} \mathbf{u}_\phi \quad (9)$$

with

$$\begin{aligned} A_{1\theta} &= a_{o(h)} \exp(+j\delta_{o(h)}) \tilde{A}_{1(vh)} + a_{o(v)} \exp(+j\delta_{o(v)}) \tilde{A}_{1(vv)} \\ A_{1\phi} &= a_{o(h)} \exp(+j\delta_{o(h)}) \tilde{A}_{1(hh)} + a_{o(v)} \exp(+j\delta_{o(v)}) \tilde{A}_{1(hv)} \end{aligned} \quad (10)$$

where $\tilde{A}_{1(ba)} = \frac{A_{1(ba)}}{L}$. To describe the polarization state of the scattered wave, we use the Stokes parameters [39],

$$S_0 = M_\theta^2 + M_\phi^2 \quad (11)$$

$$S_1 = M_\theta^2 - M_\phi^2 \quad (12)$$

$$S_2 = 2M_\theta M_\phi \cos(\Psi_\theta - \Psi_\phi) \quad (13)$$

$$S_3 = 2M_\theta M_\phi \sin(\Psi_\theta - \Psi_\phi) \quad (14)$$

where the pairs (M_θ, Ψ_θ) and (M_ϕ, Ψ_ϕ) are the modulus and phase of the complex amplitudes $A_{1(\theta)}$ and $A_{1(\phi)}$, respectively. We note $\Psi_{\theta\phi} = \Psi_\theta - \Psi_\phi$ the phase difference. For a linearly polarized scattered wave, $S_3 = 0$. For a RHC-polarized scattered wave, $M_\theta^2 = M_\phi^2$ and $\Psi_{\theta\phi} = \pi/2$. As a result, $S_1 = S_2 = 0$

and $S_0 = S_3 = 2M_\theta^2$. For a LHC-polarized scattered wave, $M_\theta^2 = M_\phi^2$ and $\Psi_{\theta\phi} = -\pi/2$ and consequently, $S_1 = S_2 = 0$ and $S_0 = -S_3 = 2M_\theta^2$.

C. Scattered amplitudes as random processes

We consider slightly rough interfaces. The first-order SPM gives the scattering amplitude $\tilde{A}_{1(ba)}$ as follows [12]-[13], [21]:

$$\tilde{A}_{1(ba)}(\alpha, \beta) = \sum_{i=1}^{N-1} K_{1(ba)}^{(1)}(\alpha, \beta) \hat{a}_i(\alpha - \alpha_0, \beta - \beta_0). \quad (15)$$

The superscript (1) refers to the first-order SPM. The function $\hat{a}_i(\alpha, \beta)$ is the 2D Fourier transform of the function $a_i(x, y)$ divided by the length L . The closed-form expressions of first-order SPM kernels $K_{1(ba)}^{(1)}(\alpha, \beta)$ were first obtained in [12] for a stratified structure with two rough interfaces. The kernels were first obtained in [13] by a recurrence relation for an arbitrary number of rough interfaces. For a stratified medium with three rough interfaces, the kernels were expressed in [25, appendix A] as functions of the relative permittivity values, the layer thicknesses, and of the incidence and scattering angles.

The interface height distributions are assumed to be centered and Gaussian. As shown by (15), the scattering amplitude $\tilde{A}_{1(ba)}^{(1)}(\alpha, \beta)$ is expressed as a linear combination of the Fourier transforms of the rough interface height profiles. Since the Fourier Transform is linear and the Gaussian character is preserved by linear operation, the scattering amplitudes $\tilde{A}_{1(ba)}^{(1)}(\alpha, \beta)$ are angular Gaussian processes. Let $R_{(ba)}$ and $I_{(ba)}$ be the real and imaginary parts of $\tilde{A}_{1(ba)}^{(1)}(\alpha, \beta)$ and let $R_{(b'a')}$ and $I_{(b'a')}$ be those of $\tilde{A}_{1(b'a')}^{(1)}(\alpha, \beta)$. We deduce that for a given direction (θ, ϕ) , the four random variables $R_{(ba)}$, $I_{(ba)}$, $R_{(b'a')}$ and $I_{(b'a')}$ follow a four-order Gaussian distribution.

Let R_θ and I_θ be the real and imaginary parts of A_θ and let R_ϕ and I_ϕ be those of A_ϕ . We find from (9)

$$\begin{aligned}
R_\theta &= \left[R_{(vh)} \cos(\delta_{o(h)}) - I_{(vh)} \sin(\delta_{o(h)}) \right] a_{o(h)} + \left[R_{(v\bar{v})} \cos(\delta_{o(v)}) - I_{(v\bar{v})} \sin(\delta_{o(v)}) \right] a_{o(v)} \\
I_\theta &= \left[I_{(vh)} \cos(\delta_{o(h)}) + R_{(vh)} \sin(\delta_{o(h)}) \right] a_{o(h)} + \left[I_{(v\bar{v})} \cos(\delta_{o(v)}) + R_{(v\bar{v})} \sin(\delta_{o(v)}) \right] a_{o(v)} \\
R_\phi &= \left[R_{(hh)} \cos(\delta_{o(h)}) - I_{(hh)} \sin(\delta_{o(h)}) \right] a_{o(h)} + \left[R_{(h\bar{v})} \cos(\delta_{o(v)}) - I_{(h\bar{v})} \sin(\delta_{o(v)}) \right] a_{o(v)} \\
I_\phi &= \left[I_{(hh)} \cos(\delta_{o(h)}) + R_{(hh)} \sin(\delta_{o(h)}) \right] a_{o(h)} + \left[I_{(h\bar{v})} \cos(\delta_{o(v)}) + R_{(h\bar{v})} \sin(\delta_{o(v)}) \right] a_{o(v)}
\end{aligned} \tag{16}$$

We deduce from (16) that the four random variables R_θ , I_θ , R_ϕ and I_ϕ also follow a four-order Gaussian distribution. Insofar as the rough surface height distributions are centered, the four random variables are also centered and the joint PDF is given by

$$p_{R_\theta I_\theta R_\phi I_\phi}(a, b, c, d) = \frac{1}{4\pi^2 \sqrt{de(\Gamma)}} \exp \left[-\frac{1}{2} (a, b, c, d) \Gamma^{-1} (a, b, c, d)^T \right] \tag{17}$$

where Γ is the covariance matrix. The symbol T denotes the transpose. As in [22], we show from (15) and (16) that when $L \rightarrow +\infty$, the covariance matrix only depends on four primary parameters: the variances $\sigma_{R_\theta}^2$ and $\sigma_{R_\phi}^2$ of random variables R_θ and R_ϕ , their covariance $\Gamma_{R_\theta R_\phi}$ and the covariance $\Gamma_{R_\theta I_\phi}$ between R_θ and I_ϕ . We obtain

$$\mathbf{\Gamma} = \begin{pmatrix} \sigma_{R_\theta}^2 & 0 & \Gamma_{R_\theta R_\phi} & \Gamma_{R_\theta I_\phi} \\ 0 & \sigma_{R_\phi}^2 & -\Gamma_{R_\theta I_\phi} & \Gamma_{R_\theta R_\phi} \\ \Gamma_{R_\theta R_\phi} & -\Gamma_{R_\theta I_\phi} & \sigma_{R_\phi}^2 & 0 \\ \Gamma_{R_\theta I_\phi} & \Gamma_{R_\theta R_\phi} & 0 & \sigma_{R_\phi}^2 \end{pmatrix}. \tag{18}$$

In the appendix A, the four primary parameters are expressed as a function of the amplitudes $a_{o(h)}$ and $a_{o(v)}$ of the h- and v-polarized components of the incident plane wave, of the phase difference δ_{vh} and of the variance $\sigma_{R_{(ba)}}^2$ of the real part of the scattered amplitude $\tilde{A}_{1(ba)}^{(1)}(\alpha, \beta)$, the covariance $\Gamma_{R_{(ba)} R_{(b'a)}}$ between the real parts of $\tilde{A}_{1(ba)}^{(1)}(\alpha, \beta)$ and $\tilde{A}_{1(b'a)}^{(1)}(\alpha, \beta)$ and the covariance $\Gamma_{R_{(ba)} I_{(b'a)}}$ between the real part of $\tilde{A}_{1(ba)}^{(1)}(\alpha, \beta)$ and the imaginary part of $\tilde{A}_{1(b'a)}^{(1)}(\alpha, \beta)$ with (a) , (b) , (a') and (b') equal to (h) or (v) . As shown in the appendix A, the variances $\sigma_{R_{(ba)}}^2$ and the covariances $\Gamma_{R_{(ba)} R_{(b'a)}}$ and $\Gamma_{R_{(ba)} I_{(b'a)}}$ are expressed as a function of first-order SPM Kernels and interface spectra. As a result, the four primary parameters are fully determined by the thickness of central layer, the relative permittivity values, the incidence and scattering angles and by the geometrical parameters of the rough boundaries.

Using polar coordinates, we derive from (17) the 4D-joint PDF of the random variables M_θ , Ψ_θ ,

M_ϕ et Ψ_ϕ and we obtain

$$P_{M_\theta \Psi_\theta M_\phi \Psi_\phi}(m_\theta, \psi_\theta, m_\phi, \psi_\phi) = \frac{m_\theta m_\phi}{4\pi^2 \sigma_{R_\theta}^2 \sigma_{R_\phi}^2 (1-r^2)} \exp \left[-\frac{1}{2(1-r^2)} \left(\frac{m_\theta^2}{\sigma_{R_\theta}^2} - 2 \frac{m_\theta m_\phi}{\sqrt{\sigma_{R_\theta}^2 \sigma_{R_\phi}^2}} \zeta + \frac{m_\phi^2}{\sigma_{R_\phi}^2} \right) \right] \quad (19)$$

with

$$\zeta = r \cos(\psi_{\theta\phi} + \psi_0). \quad (20)$$

The quantity r is the modulus of the normalized correlation coefficient between the two complex random variables $A_{1\theta}$ and $A_{1\phi}$. The quantity r is also called the degree of coherence with

$$r = \sqrt{(\Gamma_{R_\theta R_\phi}^2 + \Gamma_{R_\theta I_\phi}^2) / (\sigma_{R_\theta}^2 \sigma_{R_\phi}^2)}. \quad (21)$$

The angle ψ_0 is the argument of the complex correlation coefficient, generally called the mean effective phase difference. This reference angle is defined as follows:

$$\psi_0 = \arctan(\Gamma_{R_\theta I_\phi} / \Gamma_{R_\theta R_\phi}). \quad (22)$$

The degree of coherence and the average effective phase difference are involved in the calculation of the inverse of the covariance matrix and its determinant. According to (21)-(22) and (A1)-(A7), the degree of coherence and the average effective phase difference are fully determined by the knowledge of the geometrical and electrical parameters of the multilayered structure and of the radar configuration.

Knowing that in the incidence plane ($\phi = \phi_0$), the first-order cross-polarized amplitudes $\tilde{A}_{1(hv)}^{(1)}$ and $\tilde{A}_{1(vh)}^{(1)}$ are equal to zero, we find from (A1)-(A4) that the degree of coherence $r(\phi = \phi_0)$ depends neither on the phase difference δ_{vh} nor on the amplitudes $a_{o(h)}$ and $a_{o(v)}$ of the h- and v-polarized components of the incident plane wave with

$$r(\phi = \phi_0) = \sqrt{(\Gamma_{R_{vv}R_{hh}}^2 + \Gamma_{R_{vv}I_{hh}}^2) / (\sigma_{R_{vv}}^2 \sigma_{R_{hh}}^2)}. \quad (23)$$

Moreover, the reference angle $\Psi_0(\phi = \phi_0)$ is such that

$$\psi_0(\phi = \phi_0) + \psi_{0(vv, hh)} = \frac{\pi}{2} - \delta_{vh} \quad (24)$$

with $\psi_{0(vv, hh)} = \arctan(\Gamma_{R_{vv}I_{hh}} / \Gamma_{R_{vv}R_{hh}})$.

For an observation direction outside the incidence plane ($\phi \neq \phi_0$), the values of r and Ψ_0 depend on

the $a_{o(h)}$, $a_{o(v)}$ and δ_{vh} values. The degree of coherence lies between 0 and 1. When $r = 0$, the four random variables M_θ , Ψ_θ , M_ϕ et Ψ_ϕ are independent and their joint distribution is the product of the four marginal distributions. From (21), the case $r = 0$ occurs when $\Gamma_{R_\theta R_\phi} = \Gamma_{R_\theta I_\phi} = 0$. In the appendix B, we show that depending on the covariances $\Gamma_{R_{(ba)}R_{(b'a)}}$ and $\Gamma_{R_{(ba)}I_{(b'a)}}$, there exist two pairs $(a_{o(h)} / a_{o(v)}, \delta_{vh})$ for which the degree of coherence is zero [40], i.e., for which the zenithal and azimuthal components of the far electric field are uncorrelated.

D. Stokes parameters as random processes

The Stokes parameters are random processes depending on the angles θ and ϕ . For a given direction, they are random variables. To establish the Stokes parameter PDF, the joint PDF of M_θ , M_ϕ and $\Psi_{\theta\phi}$ may be derived as done in [32].

$$P_{M_\theta M_\phi \Psi_{\theta\phi}}(m_\theta, m_\phi, \Psi_{\theta\phi}) = \frac{m_\theta m_\phi}{2\pi\sigma_{R_\theta}^2 \sigma_{R_\phi}^2 (1-r^2)} \exp\left[-\frac{1}{2(1-r^2)}\left(\frac{m_\theta^2}{\sigma_{R_\theta}^2} - 2\frac{m_\theta m_\phi}{\sqrt{\sigma_{R_\theta}^2 \sigma_{R_\phi}^2}}\zeta + \frac{m_\phi^2}{\sigma_{R_\phi}^2}\right)\right]. \quad (25)$$

The statistic distribution of each Stoke parameter can then be deduced as a function of the four primary parameters $\sigma_{R_\theta}^2$, $\sigma_{R_\phi}^2$, $\Gamma_{R_\theta R_\phi}$ and $\Gamma_{R_\theta I_\phi}$ which depend on the first-order SPM Kernels and the interface spectra. The following section is dedicated to the determination of the closed-form expressions for the PDF, the CDF, the mean and the variance of each Stokes parameter.

III. Statistics of the Stokes parameters

A. Statistics of S_0 and S_1

Closed-form expression for the PDF of S_0 and S_1 was derived in [32]-[34] from the joint PDF $P_{M_\theta M_\phi \Psi_{\theta\phi}}$. For the PDF $p_{S_0}(s_0)$ of the non-negative random variable S_0 , the following expression was obtained

$$p_{S_0}(s_0) = \frac{1}{\sigma_{R_\theta} \sigma_{R_\phi}} \frac{1}{[(p_0 - p_0^{-1})^2 + 4r^2]^{1/2}} \exp\left[-\frac{(p_0 + p_0^{-1})s_0}{4(1-r^2)\sigma_{R_\theta} \sigma_{R_\phi}}\right] \sinh \frac{s_0 \sqrt{(p_0 - p_0^{-1})^2 + 4r^2}}{4\sigma_{R_\theta} \sigma_{R_\phi} (1-r^2)} \quad (26)$$

where $s_0 \geq 0$, $p_0 = \sigma_{R_\theta} / \sigma_{R_\phi}$ and $\sinh(\cdot)$ denotes the hyperbolic sine function. The marginal PDF $p_{S_0}(s_0)$

does not depend on ψ_0 . The first- and second-order moments were evaluated by integration of (26),

$$m_{S_0} = \int_0^{+\infty} s_0 p_{S_0}(s_0) ds_0 = 2(\sigma_{R_\phi}^2 + \sigma_{R_\theta}^2) \quad (27)$$

$$m_{S_0^2} = \int_0^{+\infty} s_0^2 p_{S_0}(s_0) ds_0 = 8\left(\sigma_{R_\theta}^4 + \sigma_{R_\phi}^4 + (1+r^2)\sigma_{R_\theta}^2 \sigma_{R_\phi}^2\right). \quad (28)$$

In [32]-[34], the authors did not determine the CDF. The CDF of the random variable S_0 is the integral of its PDF,

$$F_{S_0}(s_0) = \text{Prob}\{S_0 \leq s_0\} = \int_0^{s_0} p_{S_0}(s_0) ds_0 \quad (29)$$

and we obtain

$$F_{S_0}(s_0) = 1 - \exp\left[-\frac{(p_0 + p_0^{-1})}{4\sigma_{R_\theta}\sigma_{R_\phi}(1-r^2)} s_0\right] \left\{ \cosh\left[\frac{\sqrt{(p_0 - p_0^{-1})^2 + 4r^2}}{4\sigma_{R_\theta}\sigma_{R_\phi}(1-r^2)} s_0\right] + \frac{(p_0 + p_0^{-1})}{\sqrt{(p_0 - p_0^{-1})^2 + 4r^2}} \sinh\left[\frac{\sqrt{(p_0 - p_0^{-1})^2 + 4r^2}}{4\sigma_{R_\theta}\sigma_{R_\phi}(1-r^2)} s_0\right] \right\} \quad (30)$$

where $s_0 \geq 0$ and $\cosh(\cdot)$ denotes the hyperbolic cosine function.

For the PDF $p_{S_1}(s_1)$, the following expression was already obtained [32]-[34]:

$$p_{S_1}(s_1) = \begin{cases} \frac{1}{2\sigma_{R_\theta}\sigma_{R_\phi}c} \exp\left[s_1 \frac{c + (p_0 - p_0^{-1})}{4\sigma_{R_\theta}\sigma_{R_\phi}(1-r^2)}\right] & \text{if } s_1 < 0 \\ \frac{1}{2\sigma_{R_\theta}\sigma_{R_\phi}c} \exp\left[-s_1 \frac{c - (p_0 - p_0^{-1})}{4\sigma_{R_\theta}\sigma_{R_\phi}(1-r^2)}\right] & \text{if } s_1 \geq 0 \end{cases} \quad (31)$$

with $c = [(p_0 + p_0^{-1})^2 - 4r^2]^{1/2}$. The first- and second-order moments were evaluated by integration of

(31) with

$$m_{S_1} = \int_{-\infty}^{+\infty} s_1 p_{S_1}(s_1) ds_1 = 2(\sigma_{R_\theta}^2 - \sigma_{R_\phi}^2) \quad (32)$$

$$m_{S_1^2} = 8\left[(\sigma_{R_\theta}^4 + \sigma_{R_\phi}^4) - \sigma_{R_\theta}^2 \sigma_{R_\phi}^2 (1+r^2)\right] \quad (33)$$

The probability law $p_{S_1}(s_1)$ does not depend on ψ_0 and is centered when $\sigma_{R_\theta}^2 = \sigma_{R_\phi}^2$. As previously, the

CDF of S_1 is obtained from the integral of its PDF. After some algebraic manipulation, we find

$$F_{S_1}(s_1) = \begin{cases} \frac{1}{c} \frac{2(1-r^2)}{[c+(p_0-p_0^{-1})]} \exp\left[s_1 \frac{c+(p_0-p_0^{-1})}{4\sigma_{R_\theta}\sigma_{R_\phi}(1-r^2)} \right] & \text{if } s_1 < 0 \\ 1 - \frac{2(1-r^2)}{c[c-(p_0-p_0^{-1})]} \exp\left[-s_1 \frac{c-(p_0-p_0^{-1})}{4\sigma_{R_\theta}\sigma_{R_\phi}(1-r^2)} \right] & \text{if } s_1 > 0 \end{cases} \quad (34)$$

B. Statistics of S_2 and S_3

In [33], the probability law for the random variables S_2 and S_3 derived from the joint PDF $p_{M_\theta M_\phi \Psi_{\theta\phi}}(m_\theta, m_\phi, \Psi_{\theta\phi})$ was given as an integral which needed to be numerically evaluated. The first two moments were also obtained by numerical integrations. The calculation steps giving this integral are summarized in appendix C. In appendix D, we establish the analytical expression for the PDF $p_{S_2}(s_2)$ and we obtain

$$p_{S_2}(s_2) = \frac{\exp\left[-\frac{|s_2|\sqrt{1-r^2\sin^2(\psi_0)} - s_2 r \cos(\psi_0)}{2\sigma_{R_\theta}\sigma_{R_\phi}(1-r^2)} \right]}{4\sigma_{R_\theta}\sigma_{R_\phi}\sqrt{1-r^2\sin^2(\psi_0)}}. \quad (35)$$

After some analytical manipulations, we establish the closed-form expression for the first- and second-order moments of the random variable S_2 ,

$$m_{S_2} = \int_{-\infty}^{+\infty} s_2 p_{S_2}(s_2) ds_2 = 4r\sigma_{R_\theta}\sigma_{R_\phi}\cos(\psi_0) \quad (36)$$

$$m_{S_2^2} = 8\sigma_{R_\theta}^2\sigma_{R_\phi}^2 \left[1 - r^2\sin^2(\psi_0) + 3r^2\cos^2(\psi_0) \right]. \quad (37)$$

The PDF $p_{S_2}(s_2)$ is centered when the degree of coherence r is equal to zero or when the reference angle ψ_0 is $\pm\frac{\pi}{2}$. The CDF of S_2 is expressed as the integral of $p_{S_2}(s_2)$ and we find

$$F_{S_2}(s_2) = \begin{cases} \frac{(1-r^2)\exp\left[\frac{\sqrt{1-r^2\sin^2(\psi_0)} + r\cos(\psi_0)}{2\sigma_{R_\theta}\sigma_{R_\phi}(1-r^2)} s_2 \right]}{2\left(1-r^2\sin^2(\psi_0) + r\cos(\psi_0)\sqrt{1-r^2\sin^2(\psi_0)}\right)} & \text{if } s_2 < 0 \\ 1 - \frac{(1-r^2)\exp\left[-\frac{\sqrt{1-r^2\sin^2(\psi_0)} - r\cos(\psi_0)}{2\sigma_{R_\theta}\sigma_{R_\phi}(1-r^2)} s_2 \right]}{2\left(1-r^2\sin^2(\psi_0) - r\cos(\psi_0)\sqrt{1-r^2\sin^2(\psi_0)}\right)} & \text{if } s_2 > 0 \end{cases} \quad (38)$$

In a similar way, the PDF $p_{S_3}(s_3)$ of S_3 is obtained by integrating $p_{S_2, S_3}(s_2, s_3)$ given by (C5) over s_2 and we deduce the analytical expressions for the PDF, the CDF and the first and second-order moments by substituting $\sin(\psi_0)$ by $\cos(\psi_0)$ and $\cos(\psi_0)$ by $-\sin(\psi_0)$ into (35), (36), (37) and (38), respectively.

In particular, we obtain

$$m_{S_3} = -4r\sigma_{R_\theta}\sigma_{R_\phi}\sin(\psi_0) \quad (39)$$

$$m_{S_3^2} = 8\sigma_{R_\theta}^2\sigma_{R_\phi}^2 \left[1 - r^2 \cos^2(\psi_0) + 3r^2 \sin^2(\psi_0) \right]. \quad (40)$$

The probability law $p_{S_3}(s_3)$ is centered when the degree of coherence r is equal to zero or when the reference angle ψ_0 is equal to 0 or $\pm\pi$.

Contrary to the PDF of S_0 or S_1 , the probability law for S_2 and S_3 depends on the mean effective phase difference ψ_0 . The marginal probabilities $p_{S_2}(s_2)$ and $p_{S_3}(s_3)$ become identified with expressions obtained in [34]. To our knowledge, the derivation that we propose has not been published and is useful in terms of analytical calculation for the continuation of [33].

C. Remarks

We deduce from (11)-(14) that the second-order moments of the four Stokes parameters must obey a linear equality

$$m_{S_0^2} = m_{S_1^2} + m_{S_2^2} + m_{S_3^2}. \quad (41)$$

By substituting the second-order moments into (41), we check the equality for all values of r and ψ_0 .

The variance of the Stokes parameter S_i is obtained from the values of m_{S_i} and $m_{S_i^2}$ with $\sigma_{S_i}^2 = m_{S_i^2} - m_{S_i}^2$.

We define the normalized Stokes parameters by $\bar{S}_i = S_i / \sigma_{R_\theta}\sigma_{R_\phi}$ ($i = 0, 1, 2, 3$). The PDF of \bar{S}_i is given by

$p_{\bar{S}_i}(\bar{s}_i) = \sigma_{R_\theta}\sigma_{R_\phi} p_{S_i}(\sigma_{R_\theta}\sigma_{R_\phi}\bar{s}_i)$ and the CDF by $F_{\bar{S}_i}(\bar{s}_i) = F_{S_i}(\sigma_{R_\theta}\sigma_{R_\phi}\bar{s}_i)$. The first-moment $m_{\bar{S}_i}$ of the random

variable \bar{S}_i is equal to $m_{S_i} / \sigma_{R_\theta}\sigma_{R_\phi}$ and the second order moment $m_{\bar{S}_i^2}$, to $m_{S_i^2} / (\sigma_{R_\theta}^2\sigma_{R_\phi}^2)$, respectively.

The distribution of \bar{S}_0 or \bar{S}_1 depends on the degree of coherence r and on the ratio $p_0 = \sigma_{R_\theta} / \sigma_{R_\phi}$. The

distribution of \bar{S}_2 or \bar{S}_3 is a three-parameter distribution which also depends on the reference angle ψ_0 .

IV. Validation of the analytical expressions

We consider an air / snow cover / frozen soil / unfrozen soil structure illuminated in L band with $\lambda = 30$ cm [3]. The rough surfaces are characterized by Gaussian correlation functions with the rms-heights $\sigma_1 = 0.015\lambda$, $\sigma_2 = 0.022\lambda$ and $\sigma_3 = 0.023\lambda$ and with the correlation lengths $l_1 = \lambda/5$, $l_2 = \lambda/4$ and $l_3 = 3\lambda/10$. The three interfaces are uncorrelated. The considered vertical profile is characterized by $\varepsilon_{r1} = 1$, $\varepsilon_{r2} = 1.25 - j3.3 \times 10^{-5}$, $\varepsilon_{r3} = 5.5 - j0.5$, $\varepsilon_{r4} = 19.3 - j2.3$, $d_2 = 2\lambda$ and $d_3 = \lambda$ [3].

Table I gives the mean and the standard deviation for each normalized Stokes parameter \bar{S}_i in the backscattering direction with $\theta = -\theta_0 = -50^\circ$ and $\phi = \phi_0 = 0^\circ$. The stratified structure is illuminated by a right-handed circularly polarized plane wave with $\delta_{vh} = +\pi/2$ and $a_{o(h)} = a_{o(v)}$. The theoretical values are obtained for surfaces of infinite extent. The numerical values are, as for them, estimated over the scattered amplitudes (given by (15)) associated with 2^{13} subsurface realizations where $L = 20\lambda$. Comparison is conclusive and validates the theoretical expressions of the first- and second- order moments in the backscattering direction. Fig. 2 shows the PDF for each normalized Stokes parameter \bar{S}_i in the backscattering direction. The agreement between the theoretical probability laws with the histograms obtained from Monte Carlo simulations is very good. Fig. 3 shows the theoretical and simulated CDFs for the same configuration. Theoretical and Monte-Carlo curves are superimposed. This comparison validates the theory in the backscattering direction.

For the studied configuration, the degree of coherence r given by (21) is equal to 0.995 with $\Gamma_{R_\theta R_\phi} = -9.27 \times 10^{-6}$, $\Gamma_{R_\theta I_\phi} = 5.28 \times 10^{-6}$, $\sigma_{R_\theta}^2 = 7.60 \times 10^{-5}$ and $\sigma_{R_\phi}^2 = 3.82 \times 10^{-5}$. Therefore, the two complex amplitudes $A_{1\theta}$ and $A_{1\phi}$ are strongly correlated. The reference angle Ψ_0 given by (22) is equal to 100° . The normalized correlation coefficient is also estimated from the set of 2^{13} realizations of scattered amplitudes. The obtained value for the degree of coherence is 0.997 and for the mean effective phase difference, 99.7° , respectively. We note very small differences between theoretical values and simulation results.

Given the values of r and Ψ_0 , the probability law for each of the Stokes parameters is close to a one-sided decaying exponential function (right-sided decaying exponential for \bar{S}_0 and \bar{S}_1 and left-sided

decaying exponential for \bar{S}_2 and \bar{S}_3). As a result, the standard deviation σ_{S_i} of \bar{S}_i is close to the mean m_{S_i} . The CDF $F_{\bar{S}_1}(\bar{s}_1)$ at the origin is equal to 0.0162. This means that the modulus $M_{1\theta}$ of the complex amplitude $A_{1\theta}$ is smaller than the modulus $M_{1\phi}$ of $A_{1\phi}$ for only 1.6% of the realizations of the stratified medium (133 cases observed out of 2^{13} simulated). The CDF $F_{\bar{S}_3}(\bar{s}_3)$ at the origin is equal to 0.997. This means that the backscattered wave is elliptically polarized in the LH sense for 99.7% of the realizations of the stratified medium. Therefore, in 0.0293% of cases, the backscattered wave is elliptically polarized in the RH sense (24 cases observed out of 2^{13} simulated). When the stratified medium is illuminated by a left-handed circularly polarized plane wave with $\delta_{ih} = -\pi/2$ and $a_{o(h)} = a_{o(v)}$, we find the same value of r and $\Psi_0 = +280^\circ$ as predicted by (23) and (24). As a result, for the Stokes parameters \bar{S}_0 and \bar{S}_1 , the PDF is unchanged. For the Stokes parameters \bar{S}_2 and \bar{S}_3 , the PDF is obtained from the graph shown in fig.2 by symmetric with respect to the Oy-axis.

TABLE I
MEAN AND STANDARD DEVIATION OF NORMALIZED STOKES PARAMETERS
FOR $\theta = -\theta_0 = -50^\circ$, $\phi = \phi_0 = 0^\circ$ AND A RHC INCIDENT POLARIZATION

Parameter		\bar{S}_0	\bar{S}_1	\bar{S}_2	\bar{S}_3
Theory	Mean	4.24	1.40	-0.689	-3.92
	STD	4.23	1.43	0.741	3.93
Monte-Carlo	Mean	4.24	1.41	-0.686	-3.92
	STD	4.20	1.42	0.743	3.90

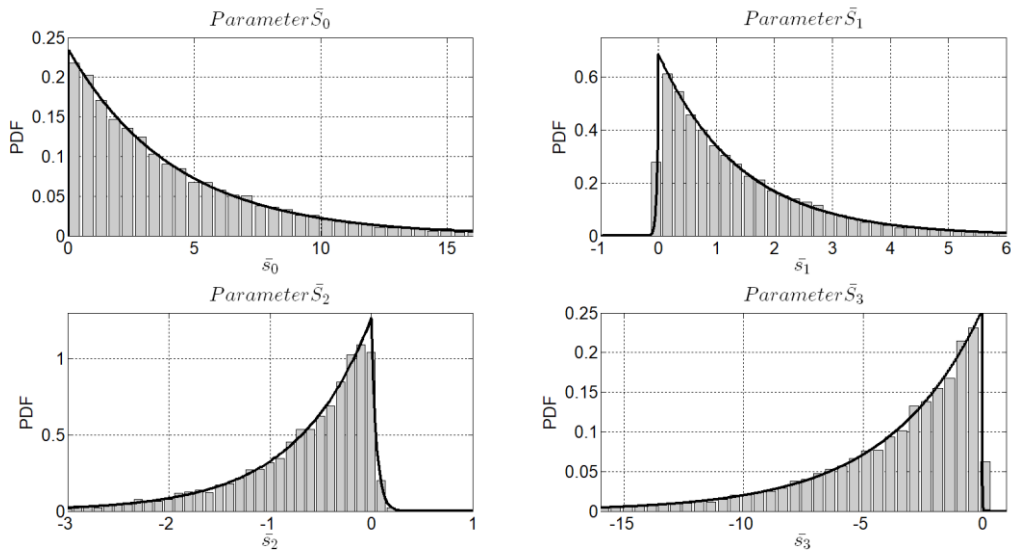


Fig. 2. Theoretical PDF and normalized histogram for each normalized Stokes parameter with $\theta = -\theta_0 = -50^\circ$, $\phi = \phi_0 = 0^\circ$ and a RHC incident polarization.

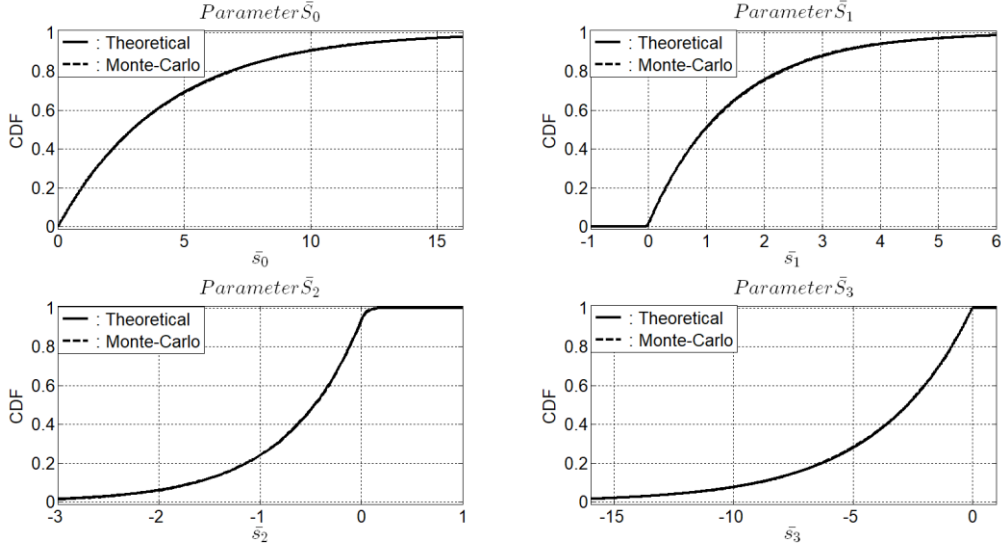


Fig. 3. Theoretical CDF and CDF estimated from Monte-Carlo simulations for each normalized Stokes parameter with $\theta = -\theta_0 = -50^\circ$, $\phi = \phi_0 = 0^\circ$ and a RHC incident polarization.

Table II gives the mean and the standard deviation for each normalized Stokes parameter \bar{S}_i in the observation direction $(\theta, \phi) = (50^\circ, 45^\circ)$. The stratified structure is illuminated by a RHC-polarized plane wave under the incidence angles $\theta_0 = 50^\circ$ and $\phi_0 = 0^\circ$. Comparison between the theoretical values and the simulated ones is conclusive. Fig. 4 shows the associated PDFs and Fig.5, the CDFs, respectively. The agreement is very good. For the studied configuration, the degree of coherence r given by (21) is equal to 0.987 with $\Gamma_{R_\theta R_\phi} = 3.24 \times 10^{-5}$, $\Gamma_{R_\theta I_\phi} = 1.11 \times 10^{-4}$, $\sigma_{R_\theta}^2 = 9.17 \times 10^{-5}$ and $\sigma_{R_\phi}^2 = 1.50 \times 10^{-4}$. The two components $A_{1\theta}$ and $A_{1\phi}$ of the scattered signal are strongly correlated. The reference angle Ψ_0 given by (22) is equal to 73.7° . The values estimated from the set of realizations are close to the theoretical ones with $r = 0.996$ and $\Psi_0 = 73.6^\circ$. Given the values of r and Ψ_0 , as previously, the probability law for each of the normalized Stokes parameters is close to a one-sided decaying exponential function (here, right-sided decaying exponential for the Stokes parameters \bar{S}_0 and \bar{S}_2 and left-sided decaying exponential for \bar{S}_1 and \bar{S}_3) and the standard deviation σ_{S_i} of \bar{S}_i is close to the mean m_{S_i} . The CDF $F_{\bar{S}_1}(\bar{S}_1)$ at the origin is equal to 0.921. This means that the modulus $M_{1\theta}$ of the complex amplitude $A_{1\theta}$ is smaller than the modulus $M_{1\phi}$ of $A_{1\phi}$ for 92.1% of the realizations of the stratified medium (7545 cases observed out of 2^{13} simulated). The CDF $F_{\bar{S}_3}(\bar{S}_3)$ at the origin is equal to

0.993. The scattered wave is therefore elliptically polarized in the LH sense for 99.3% of the realizations of the stratified medium and for 0.0707% of cases, the scattered wave is elliptically polarized in the RH sense (58 cases observed out of 2^{13} simulated).

TABLE 2
MEAN AND STANDARD DEVIATION OF NORMALIZED STOKES PARAMETER IN THE OBSERVATION DIRECTION
 $(\theta, \phi) = (50^\circ, 45^\circ)$ AND AN ILLUMINATION BY A RHC-POLARIZED PLANE WAVE WITH $(\theta_0, \phi_0) = (50^\circ, 0^\circ)$

Parameter		\bar{S}_0	\bar{S}_1	\bar{S}_2	\bar{S}_3
Theory	Mean	4.12	-0.990	1.11	-3.80
	STD	4.10	1.09	1.20	3.82
Monte-Carlo	Mean	4.13	-0.994	1.12	-3.79
	STD	4.04	1.08	1.20	3.76

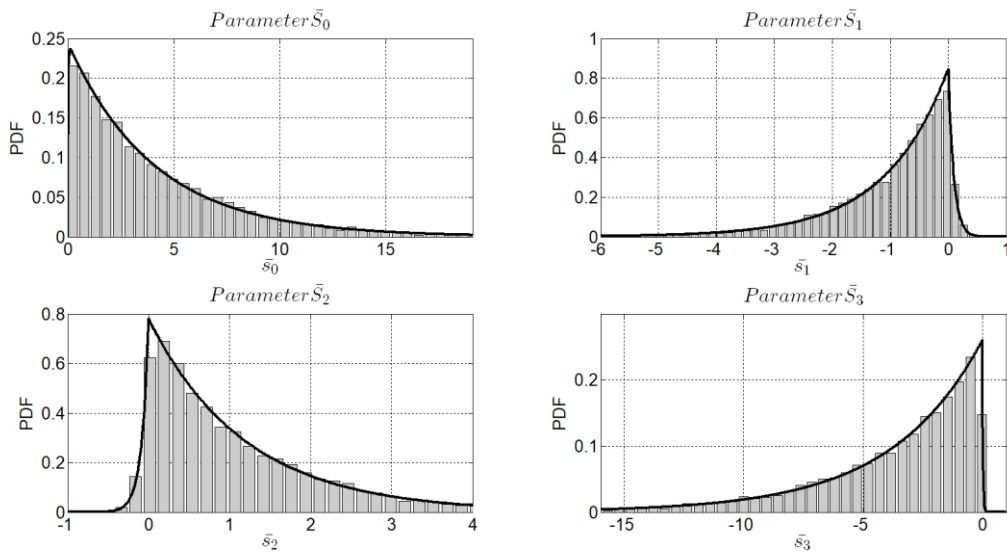


Fig. 4. Theoretical PDF and normalized histogram for normalized Stokes parameters with $(\theta, \phi) = (50^\circ, 45^\circ)$, $(\theta_0, \phi_0) = (50^\circ, 0^\circ)$ and a RHC incident polarization.

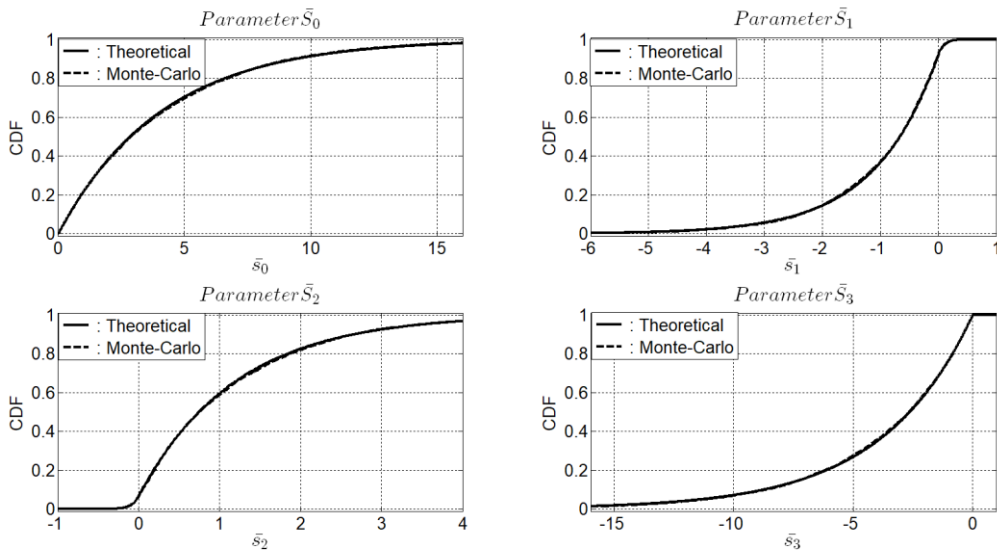


Fig. 5. Theoretical CDF and CDF estimated from Monte-Carlo simulations for each normalized Stokes parameters with $(\theta, \phi) = (50^\circ, 45^\circ)$, $(\theta_0, \phi_0) = (50^\circ, 0^\circ)$ and a RHC incident polarization.

For an observation direction in the incidence plane, the degree of coherence r does not depend on the phase difference δ_{vh} nor on the $a_{o(h)}$ and $a_{o(v)}$ amplitude values of the h- and v-polarized components of the incident plane wave. For an observation direction outside the plane of incidence, the values of r and Ψ_0 depend on the $a_{o(h)}$, $a_{o(v)}$ and δ_{vh} values. For the incidence angles $(\theta_0, \phi_0) = (50^\circ, 0^\circ)$ and the observation angles $(\theta, \phi) = (50^\circ, 45^\circ)$, we derive from expressions established in the appendix B the ratio $\rho_0 = a_{o(h)} / a_{o(v)}$ and the associated phase difference δ_{vh} for which the degree of coherence is equal to zero. We find two pairs $(\rho_0; \delta_{(vh)})$: $(1.02; 184^\circ)$ and $(0.500; 359^\circ)$. Because the phase difference is nearly equal to 180° in the first case and 360° in the second case, the incident wave is linearly polarized (in first approach). Fig. 6 shows the degree of coherence r , the reference angle ψ_0 and the ratio $p_0 = \sigma_{R_\theta} / \sigma_{R_\phi}$ (i.e., quantities which define the probability laws of the four Stokes parameters) as a function of the phase difference δ_{vh} for $a_{o(h)} = 1.02a_{o(v)}$ (left column) and $a_{o(h)} = 0.500a_{o(v)}$ (right column). When $\rho_0 = 1.02$, the degree of coherence is less than 0.5 over an angular range of 3° . When $\rho_0 = 0.500$, the angular range is 23° . The variations of ψ_0 are very marked near the phase shift δ_{vh} for which the degree of polarization is equal to zero. For two values of δ_{vh} , the parameter p_0 is equal to 1 and the standard deviations of the zenithal and azimuthal components of the scattering signal are equal.

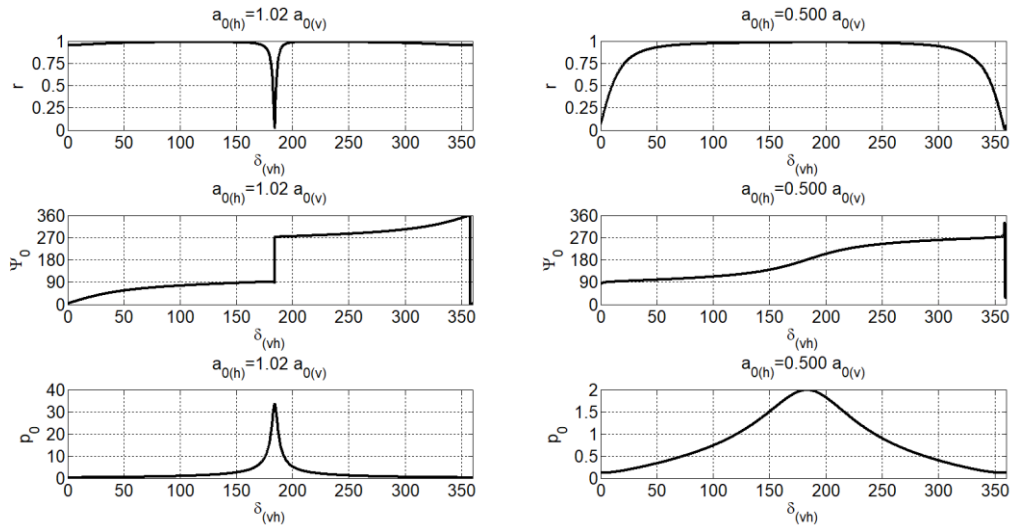


Fig. 6. Parameters r , ψ_0 and p_0 versus phase difference δ_{vh} for $a_{o(h)} = 1.08a_{o(v)}$ (left column) and $a_{o(h)} = 0.500a_{o(v)}$ (right column) with $(\theta, \phi) = (50^\circ, 45^\circ)$ and $(\theta_0, \phi_0) = (50^\circ, 0^\circ)$.

Fig. 7 shows the PDF for each normalized Stokes parameter for three values of the phase difference δ_{vh} and $a_{o(h)} = 0.500a_{o(v)}$. The values of the degree of coherence r , the reference angle ψ_0 and the ratio $p_0 = \sigma_{R_\theta} / \sigma_{R_\phi}$ are given in Table III. For $\delta_{vh} = 0^\circ$, the degree of coherence is near zero. As a result, the means $m_{\bar{S}_2}$ and $m_{\bar{S}_3}$ are close to zero and the distributions of \bar{S}_2 and \bar{S}_3 are centered. For $\delta_{vh} = 120^\circ$, the standard deviations of the zenithal and azimuthal components of the scattering signal are almost equal to 1 with $p_0 = 0.983$ and Fig.7 shows a centered distribution for the normalized Stokes parameter \bar{S}_1 . For a direction of observation outside the incidence plane, the curves of Fig.7 show that the distribution of each of the normalized Stokes parameters depends closely on the polarization state of the incident wave. The marginal probabilities in Fig. 7 were compared to the normalized histograms obtained by simulations. The comparison was conclusive but not shown here.

TABLE III

VALUES OF THE PARAMETERS r , ψ_0 AND p_0 FOR THREE VALUES OF THE PHASE DIFFERENCE δ_{vh}
WITH $(\theta, \phi) = (50^\circ, 45^\circ)$, $(\theta_0, \phi_0) = (50^\circ, 0^\circ)$ and $a_{o(h)} = 0.500a_{o(v)}$

Parameter	r	ψ_0	p_0
$\delta_{vh} = 0^\circ$	0.0577	78.9°	0.115
$\delta_{vh} = 30^\circ$	0.843	93.2°	0.217
$\delta_{vh} = 120^\circ$	0.978	120°	0.983

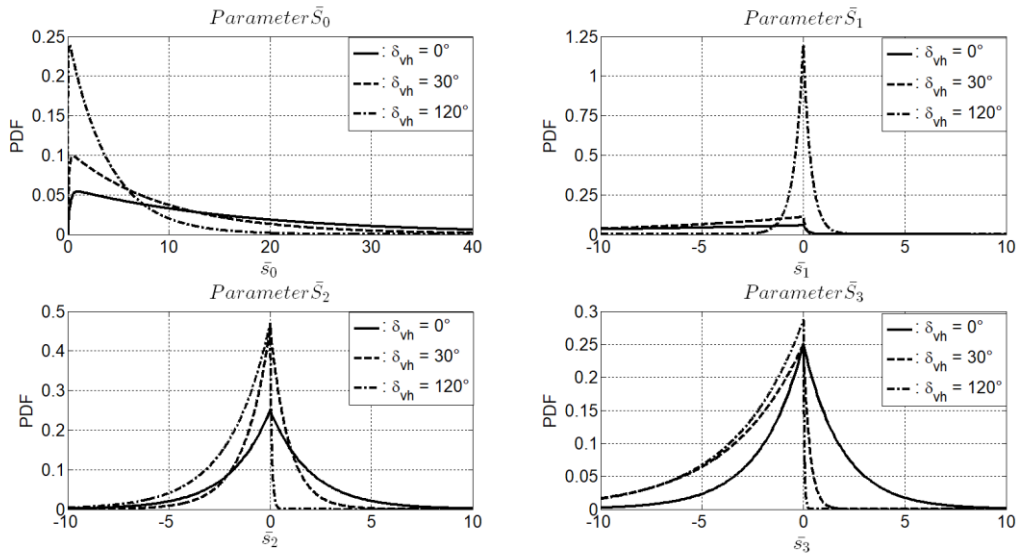


Fig. 7. Theoretical PDF for each normalized Stokes parameter with $(\theta, \phi) = (50^\circ, 45^\circ)$, $(\theta_0, \phi_0) = (50^\circ, 0^\circ)$ and $a_{o(h)} = 0.500a_{o(v)}$ and three values of the phase difference δ_{vh} .

Conclusion

In this paper, we analytically determine the statistics of the four Stokes parameters for the signal scattered by layered structures with an arbitrary number of slightly rough interfaces. The layered structure is illuminated by a monochromatic wave of an arbitrary polarization. The zenithal and azimuthal components of the far scattered electric field are derived from the first-order Small Perturbation Method. For randomly rough interfaces with infinite extensions and centred Gaussian height distributions, we show that the underlying complex scattered amplitudes follow a multivariate Gaussian model. For the Stokes vector coordinates, we establish the analytical expressions of the probability density function given by (26), (31), and (35), the cumulative density function (30), (34), and (38) and the first- and second-order moments (27)-(28), (32)-(33), (36)-(37) and (39)-(40). We also derive the statistics of the normalized Stokes parameters $\bar{S}_i = S_i / \sigma_{R_\theta} \sigma_{R_\phi}$ ($i = 0, 1, 2, 3$) where the quantities σ_{R_θ} and σ_{R_ϕ} are the standard deviations of the real part of the zenithal and azimuthal components of the scattered field. The marginal distribution for \bar{S}_0 and \bar{S}_1 depends on the degree of coherence r (i.e., the modulus of the normalized complex correlation coefficient between the two orthogonal components) and on the ratio $p_0 = \sigma_{R_\theta} / \sigma_{R_\phi}$. The marginal distribution for \bar{S}_2 or \bar{S}_3 is a three-parameter distribution that also depends on the mean effective phase difference ψ_0 (i.e., the argument of the complex correlation coefficient). We also obtain an analytical formula for the degree of coherence, the mean effective phase difference and the ratio p_0 as a function of the first-order SPM kernels, of the interface spectra and of the incidence and observations angles.

Knowing that in the incidence plane, the first-order cross-polarized amplitudes are equal to zero, we show that for a given observation direction, the degree of coherence does not depend on the phase difference and on the amplitudes of the h- and v-polarized components of the incident plane wave. For an observation direction outside the incidence plane, we define the condition on the incidence wave parameters for which the zenithal and azimuthal components are uncorrelated, i.e. for which the degree of coherence is equal to zero.

For an air / snow cover / frozen soil / unfrozen soil structure, we analyze the marginal probabilities of the Stokes parameters and validate the theory by comparison with Monte-Carlo simulations. The

stratified medium is studied in the backscattering direction and also in any observation direction. The theory assumes slightly rough surfaces with infinite extent. Nevertheless, we observe from Monte-Carlo simulations that the obtained analytical formulas are still valid for surfaces of a few hundred wavelengths squared. The agreement between simulated data and theory is observed to be very good for the PDF, the CDF, the mean, and the standard deviation. We considered random processes with Gaussian spectra but the marginal probability laws presented in this paper can be used for any finite memory random process and in the case of correlated interfaces: only the parameters of the probability laws change. Under the condition that the real and imaginary parts of the two orthogonal components of the field scattered by the illuminated zone are Gaussian random variables, these statistics of the Stokes parameters offer possibilities for in-depth investigating the polarization of scattering processes from random media.

The case of multilook data is of relevance for applications. The statistics of the Stokes parameters for multilook returns were derived in [33]. An analytical expression of the marginal probability was obtained for the two first Stokes parameters. For the two other multilook Stokes parameters, the probability law was in the form of an integral which needed to be numerically evaluated. In [42], under some reasonable approximations validated by real SAR returns, the PDFs were formulated analytically with dependence on the look number and mean values of the Stokes parameters. Rigorous analytical calculation still deserves to be performed and the statistics of multilook signatures for multilayered structures with an arbitrary number of slightly rough interfaces could be studied in this way.

Appendix A: Expressions of the four primary parameters

When $L \rightarrow +\infty$, the covariance matrix only depends on the four primary parameters : the variances $\sigma_{R_\theta}^2$ and $\sigma_{R_\phi}^2$, and the covariances $\Gamma_{R_\theta R_\phi}$ and $\Gamma_{R_\theta I_\phi}$. We derive from (16) the closed-form expressions of these variances and covariances as follows:

$$\sigma_{R_\theta}^2 = \sigma_{R_{(vh)}}^2 a_{o(h)}^2 + \sigma_{R_{(vv)}}^2 a_{o(v)}^2 + 2 \left[\Gamma_{R_{(vh)} R_{(vv)}} \cos(\delta_{vh}) + \Gamma_{R_{(vv)} I_{(vh)}} \sin(\delta_{vh}) \right] a_{o(h)} a_{o(v)} \quad (\text{A1})$$

$$\sigma_{R_\phi}^2 = \sigma_{R_{(hh)}}^2 a_{o(h)}^2 + \sigma_{R_{(hv)}}^2 a_{o(v)}^2 + 2 \left[\Gamma_{R_{(hh)} R_{(hv)}} \cos(\delta_{vh}) - \Gamma_{R_{(hh)} I_{(hv)}} \sin(\delta_{vh}) \right] a_{o(h)} a_{o(v)} \quad (\text{A2})$$

$$\Gamma_{R_\theta R_\phi} = \Gamma_{R_{(vh)R_{(hh)}}} a_{o(h)}^2 + \Gamma_{R_{(vv)R_{(hv)}}} a_{o(v)}^2 + \left[(\Gamma_{R_{(vv)R_{(hh)}}} + \Gamma_{R_{(vh)R_{(hv)}}}) \cos(\delta_{vh}) + (\Gamma_{R_{(vv)I_{(hh)}}} - \Gamma_{R_{(vh)I_{(hv)}}}) \sin(\delta_{vh}) \right] a_{o(h)} a_{o(v)} \quad (\text{A3})$$

$$\Gamma_{R_\theta I_\phi} = \Gamma_{R_{(vh)I_{(hh)}}} a_{o(h)}^2 + \Gamma_{R_{(vv)I_{(hv)}}} a_{o(v)}^2 + \left[(\Gamma_{R_{(vv)I_{(hh)}}} + \Gamma_{R_{(vh)I_{(hv)}}}) \cos(\delta_{vh}) + (\Gamma_{R_{(vh)R_{(hv)}}} - \Gamma_{R_{(vv)R_{(hh)}}}) \sin(\delta_{vh}) \right] a_{o(h)} a_{o(v)} \quad (\text{A4})$$

The variances $\sigma_{R_{(ba)}}^2$ and the covariances $\Gamma_{R_{(ba)R_{(b'a)'}}$ and $\Gamma_{R_{(ba)I_{(b'a)'}}$ are established from (15) and calculation details are given in [21-22]. We obtain

$$\sigma_{R_{(ba)}}^2 = \frac{1}{2} \sum_{i=1}^{N-1} |K_{i,ba}|^2 \hat{R}_{ii}(\alpha - \alpha_0, \beta - \beta_0) \quad (\text{A5})$$

$$\Gamma_{R_{(ba)R_{(b'a)'}} = \frac{1}{2} \sum_{i=1}^{N-1} \text{Re}[K_{i,ba}^* K_{i,b'a'} \hat{R}_{ii}(\alpha - \alpha_0, \beta - \beta_0)] \quad (\text{A6})$$

$$\Gamma_{R_{(ba)I_{(b'a)'}} = \frac{1}{2} \sum_{i=1}^{N-1} \text{Im}[K_{i,ba}^* K_{i,b'a'} \hat{R}_{ii}(\alpha - \alpha_0, \beta - \beta_0)] \quad (\text{A7})$$

Appendix B: Cases where the degree of coherence is zero

The case $r = 0$ occurs when $\Gamma_{R_\theta R_\phi} = \Gamma_{R_\theta I_\phi} = 0$. From (21) and (22), we find the following matrix equation

$$\begin{pmatrix} \cos(\delta_{vh}) \\ \sin(\delta_{vh}) \end{pmatrix} = \begin{bmatrix} g_{11} & g_{12} \\ g_{21} & g_{22} \end{bmatrix} \begin{pmatrix} \rho_0 \\ 1/\rho_0 \end{pmatrix} \quad (\text{B1})$$

with

$$\begin{bmatrix} g_{11} & g_{12} \\ g_{21} & g_{22} \end{bmatrix} = - \begin{bmatrix} \Gamma_{R_{(vv)R_{(hh)}}} + \Gamma_{R_{(vh)R_{(hv)}}} & \Gamma_{R_{(vv)I_{(hh)}}} - \Gamma_{R_{(vh)I_{(hv)}}} \\ \Gamma_{R_{(vv)I_{(hh)}}} + \Gamma_{R_{(vh)I_{(hv)}}} & \Gamma_{R_{(vh)R_{(hv)}}} - \Gamma_{R_{(vv)R_{(hh)}}} \end{bmatrix}^{-1} \begin{bmatrix} \Gamma_{R_{(vh)R_{(hh)}}} & \Gamma_{R_{(vv)R_{(hv)}}} \\ \Gamma_{R_{(vh)I_{(hh)}}} & \Gamma_{R_{(vv)I_{(hv)}}} \end{bmatrix} \quad (\text{B2})$$

and

$$\rho_0 = \frac{a_{0(h)}}{a_{0(v)}}. \quad (\text{B3})$$

Knowing that $\cos^2(\delta_{vh}) + \sin^2(\delta_{vh}) = 1$, we obtain a quadratic equation

$$c_1(\rho_0^2)^2 + c_2(\rho_0^2) + c_3 = 0 \quad (\text{B4})$$

with

$$\begin{aligned} c_1 &= g_{11}^2 + g_{21}^2 \\ c_2 &= 2(g_{11}g_{12} + g_{21}g_{22}) - 1 \\ c_3 &= g_{12}^2 + g_{22}^2 \end{aligned} \quad (\text{B5})$$

If the discriminant Δ of the quadratic equation is positive and if $c_2 < -\sqrt{\Delta}$, there are two distinct ratios

ρ_{01} and ρ_{02} for which the degree of coherence r is equal to zero and we find

$$\rho_{01} = \sqrt{\frac{-c_2 - \sqrt{\sqrt{c_2^2 - c_1 c_3}}}{2c_1}} ; \rho_{02} = \sqrt{\frac{-c_2 + \sqrt{\sqrt{c_2^2 - c_1 c_3}}}{2c_1}} \quad (\text{B6})$$

The phase difference associated with each of the two ratios is deduced from (B1).

Appendix C: The marginal PDF for the Stokes parameters S_2 and S_3 as an integral numerically evaluated

Calculation of the marginal PDF for the Stokes parameters S_2 and S_3 requires the derivation of the joint PDF of the product $V = 2M_\theta M_\phi$ and the phase difference $\Psi_{\theta\phi}$. In [33], the joint PDF $p_{V\Psi_{\theta\phi}}(v, \Psi_{\theta\phi})$ is expressed as an integral of $p_{M_\theta M_\phi \Psi_{\theta\phi}}(m_\theta, m_\phi, \Psi_{\theta\phi})$:

$$p_{V\Psi_{\theta\phi}}(v, \Psi_{\theta\phi}) = \int_0^{+\infty} p_{M_\theta M_\phi \Psi_{\theta\phi}}\left(m_\theta, \frac{v}{2m_\theta}, \Psi_{\theta\phi}\right) \frac{dm_\theta}{2m_\theta} \quad (\text{C1})$$

Substituting (25) into (C1), after some algebraic manipulations, the following expression is established

$$p_{V\Psi_{\theta\phi}}(v, \Psi_{\theta\phi}) = \frac{v}{8\pi\sigma_{R_\theta}^2 \sigma_{R_\phi}^2 (1-r^2)} \exp\left[\frac{\zeta}{2(1-r^2)\sqrt{\sigma_{R_\theta}^2 \sigma_{R_\phi}^2}} v\right] \times \int_0^{+\infty} \frac{1}{m_\theta} \exp\left[-\frac{1}{2(1-r^2)} \left(\frac{m_\theta^2}{\sigma_{R_\theta}^2} + \frac{v^2}{4m_\theta^2} \frac{1}{\sigma_{R_\phi}^2}\right)\right] dm_\theta \quad (\text{C2})$$

where ζ is given by (27). By using the modified Bessel function K_0 given by the following integral [41, p.183, (15)],

$$K_0(z) = \frac{1}{2} \int_0^{+\infty} \frac{1}{\tau} \exp\left(-\tau - \frac{z^2}{4\tau}\right) d\tau \quad (\text{C3})$$

the joint probability law $p_{V\Psi_{\theta\phi}}(v, \Psi_{\theta\phi})$ is given by

$$p_{V\Psi_{\theta\phi}}(v, \Psi_{\theta\phi}) = \frac{v}{8\pi\sigma_{R_\theta}^2 \sigma_{R_\phi}^2 (1-r^2)} \exp\left[\frac{\zeta}{2(1-r^2)\sqrt{\sigma_{R_\theta}^2 \sigma_{R_\phi}^2}} v\right] K_0\left[\frac{v}{2\sigma_{R_\theta} \sigma_{R_\phi} (1-r^2)}\right]. \quad (\text{C4})$$

Given that $S_2 = V \cos(\Psi_{\theta\phi})$ and $S_3 = V \sin(\Psi_{\theta\phi})$, knowing that the magnitude of the Jacobian of the

bijjective transformation from S_2 and S_3 to V and $\Psi_{\theta\phi}$ is equal to ν and by substituting (20) into (C4),

the joint PDF of S_2 and S_3 is obtained

$$p_{S_2, S_3}(s_2, s_3) = \frac{1}{8\pi\sigma_{R_\theta}^2\sigma_{R_\phi}^2(1-r^2)} \exp\left[\frac{s_2 r \cos(\psi_0) - s_3 r \sin(\psi_0)}{2\sigma_{R_\theta}\sigma_{R_\phi}(1-r^2)}\right] K_0\left(\frac{\sqrt{s_2^2 + s_3^2}}{2\sigma_{R_\theta}\sigma_{R_\phi}(1-r^2)}\right) \quad (C5)$$

The PDF of S_2 is obtained by integrating $p_{S_2, S_3}(s_2, s_3)$ over s_3 with

$$p_{S_2}(s_2) = \int_{-\infty}^{+\infty} p_{S_2, S_3}(s_2, s_3) ds_3 = \frac{1}{8\pi\sigma_{R_\theta}^2\sigma_{R_\phi}^2(1-r^2)} \exp\left[\frac{s_2 r \cos(\psi_0)}{2\sigma_{R_\theta}\sigma_{R_\phi}(1-r^2)}\right] \times \int_{-\infty}^{+\infty} \exp\left[\frac{-s_3 r \sin(\psi_0)}{2\sigma_{R_\theta}\sigma_{R_\phi}(1-r^2)}\right] K_0\left(\frac{\sqrt{s_2^2 + s_3^2}}{2\sigma_{R_\theta}\sigma_{R_\phi}(1-r^2)}\right) ds_3 \quad (C6)$$

In a similar way, the PDF $p_{S_3}(s_3)$ of S_3 is obtained by integrating $p_{S_2, S_3}(s_2, s_3)$ over s_2 . In [33], the integral was numerically evaluated.

Appendix D: The closed-form expression of the PDF for the Stokes parameter S_2

In this appendix, we show that the analytical calculation of $p_{S_2}(s_2)$ can be continued by substituting (C3) in (C6),

$$p_{S_2}(s_2) = \frac{1}{8\pi\sigma_{R_\theta}^2\sigma_{R_\phi}^2(1-r^2)} \exp[s_2 a_0 r \cos(\psi_0)] \times \int_0^{+\infty} \int_{-\infty}^{+\infty} \exp\left[-\frac{a_0^2 s_3^2}{4\tau} - s_3 a_0 r \sin(\psi_0)\right] ds_3 \exp\left(-\tau - \frac{a_0^2 s_2^2}{4\tau}\right) \frac{d\tau}{2\tau} \quad (D1)$$

with $a_0 = \frac{1}{2\sigma_{R_\theta}\sigma_{R_\phi}(1-r^2)} > 0$. Knowing that the integral of a Gaussian distribution over the entire real

line is equal to the unity, we show that

$$\int_{-\infty}^{+\infty} \exp\left[-\frac{a_0^2 s_3^2}{4\tau} - s_3 a_0 r \sin(\psi_0)\right] ds_3 = \frac{2\sqrt{\pi\tau}}{a_0} \exp\left[r^2 \tau \sin^2(\psi_0)\right] \quad (D2)$$

and, we deduce the PDF $p_{S_2}(s_2)$ with

$$p_{S_2}(s_2) = \frac{1}{8\pi\sigma_{R_\theta}^2\sigma_{R_\phi}^2(1-r^2)} \frac{\sqrt{\pi}}{a_0\sqrt{1-r^2\sin^2(\psi_0)}} \exp[s_2 a_0 r \cos(\psi_0)] \times \int_0^{+\infty} \exp\left(-\tau' - \frac{a_0^2[1-r^2\sin^2(\psi_0)]s_2^2}{4\tau'}\right) \frac{d\tau'}{\sqrt{\tau'}} \quad (\text{D3})$$

where $\tau' = \tau[1-r^2\sin^2(\psi_0)]$. By using the formula (D4) deduced from [41, p.183, (15)] and [41, p. 79, (8)],

$$\int_0^{+\infty} \exp\left(-\tau - \frac{z^2}{4\tau}\right) \frac{d\tau}{\sqrt{\tau}} = \sqrt{2|z|} K_{1/2}(|z|) \quad (\text{D4})$$

and knowing that [41, p.80, (13)],

$$\sqrt{|z|} K_{1/2}(|z|) = \sqrt{\frac{\pi}{2}} e^{-|z|} \quad (\text{D5})$$

we obtain the closed-form expression for the PDF $p_{S_2}(s_2)$ given by (35).

References

- [1] A. Tabatabaenejad and M. Moghaddam, "Inversion of subsurface properties of layered dielectric structures with random slightly rough interfaces using the method of simulated annealing," *IEEE Trans. Geosci. Remote Sens.*, vol. 47, no. 7, pp. 2035-2046, Jul. 2009.
- [2] B. Rabus, H. Wehn, and M. Nolan, "The importance of soil moisture and soil structure for InSAR phase and backscatter, as determined by FDTD modeling," *IEEE Trans. Geosci. Remote Sens.*, vol. 48, no. 5, pp. 2421-2429, May 2010.
- [3] M. Schwank *et al*, "Model for microwave emission of a snow-covered ground with focus on L band," *Remote Sens. Environ.* 154, pp. 180–191, Nov. 2014.
- [4] P.N. Dagurova, T.N. Chimitdorzhieva, A.V. Dmitriev and S.I. Dobrynin, "Estimation of snow water equivalent from L-band radar interferometry: simulation and experiment," *Int. J. Remote Sens.*, vol 41, no. 24, pp. 9328-9359, Oct. 2020.
- [5] R.T. Tonboe, L.T. Pedersen, and C. Haas, "Simulation of satellite radar altimeter sea ice thickness retrieval uncertainty", *Cryosphere Discuss.* 3, pp. 513–559, Jul. 2009.
- [6] R. Dusséaux, S. Afifi, and M. Dechambre, "Scattering properties of a stratified air/snow/sea ice

- medium. Small slope approximation,” *Comptes Rendus Phys.* 17, pp. 995–1002, Nov. 2016.
- [7] F. Nunziata, A. Gambardella, and M. Migliaccio, “On the Mueller scattering matrix for SAR sea oil slick observation,” *IEEE Trans. Geosci. Remote Sens. Lett.*, vol. 5, no. 4, pp. 691–695, Oct. 2008.
- [8] H. Zheng, J. Zhang, Y. Zhang, A. Khenchaf and Y. Wang, “Theoretical study on microwave scattering mechanisms of sea surfaces covered with and without oil film for incidence angle smaller than 30° ,” *IEEE Trans. Geosci. Remote Sens.*, vol.59, no 1, pp. 37-46, Jan. 2021.
- [9] C. Bourlier, N. Pinel, and G Kubické, *Method of moments for 2D scattering problems: basic concepts and applications*. Hoboken, NJ, USA: Wiley, 2013.
- [10] P. Imperatore, A. Iodice, M. Pastorino, and N. Pinel, “Modelling scattering of electromagnetic waves in layered media: An up-to-date perspective,” *Int. J. Antennas Propag.*, Nov. 2017.
- [11] F. Jonard, F. André, N. Pinel, C. Warren, H. Vereecken, and S. Lambot, “Modeling of multilayered media Green’s functions with rough interfaces,” *IEEE Trans. Geosci. Remote Sens.*, vol. 57, no. 10, pp. 7671–7681, Oct. 2019.
- [12] A. Tabatabaenejad and M. Moghaddam, “Bistatic scattering from three dimensional layered rough surfaces,” *IEEE Trans. Geosci. Remote Sens.*, vol. 44, no. 8, pp. 2102–2114, Aug. 2006.
- [13] P. Imperatore, A. Iodice, and D. Riccio, “Electromagnetic wave scattering from layered structures with an arbitrary number of rough interfaces,” *IEEE Trans. Geosci. Remote Sens.*, vol. 47, no. 4, pp. 1056–1072, Apr. 2009.
- [14] S. Afifi, R. Dusséaux, and A. Berrouk, “Electromagnetic scattering from 3D layered structures with randomly rough interfaces: Analysis with the small perturbation method and the small slope approximation,” *IEEE Trans. Antennas Propag.*, vol. 62, no. 10, pp. 5200–5208, Oct. 2014.
- [15] M. A. Demir, J. T. Johnson, and T. J. Zajdel, “A study of the fourth-order small perturbation method for scattering from two-layer rough surfaces,” *IEEE Trans. Geosci. Remote Sens.*, vol. 50, no. 9, pp. 3374–3382, Sep. 2012.
- [16] H. Zamani, A. Tavakoli, and M. Dehmollaian, “Second-order perturbative solution of scattering from two rough surfaces with arbitrary dielectric profiles,” *IEEE Trans. Antennas Propag.*, vol. 63, no. 12, pp. 5767–5776, Dec. 2015.
- [17] H. Zamani, A. Tavakoli, and M. Dehmollaian, “Scattering from layered rough surfaces: Analytical

and numerical investigations,” *IEEE Trans. Geosci. Remote Sens.*, vol. 54, no. 6, pp. 3685–3696, Jun. 2016.

[18] C. Wu and X. Zhang, “Second-order perturbative solutions for 3-D electromagnetic radiation and propagation in a layered structure with multilayer rough interfaces,” *IEEE J. Selected Topics Appl. Earth Observ. Remote Sens.*, vol. 8, no. 1, pp. 180 – 194, Jan. 2015.

[19] J. M. Soto-Crespo, M. Nieto-Vesperinas, and A. T. Friberg, “Scattering from slightly rough random surfaces: A detailed study on the validity of the small perturbation method,” *J. Opt. Soc. Amer. A*, vol. 7, no. 7, pp. 1185–1201, Jul. 1990.

[20] A. Tabatabaenejad and M. Moghaddam, “Study of validity region of small perturbation method for two-layer rough surfaces,” *IEEE Geosci. Remote Sens. Lett.*, vol. 7, no. 2, pp. 319–323, Apr. 2010.

[21] S. Afifi and R. Dusséaux, “Scattering by anisotropic rough layered 2D interfaces,” *IEEE Trans. Antennas Propag.*, vol. 60, no. 11, pp. 5315–5328, Nov. 2012.

[22] S. Afifi and R. Dusséaux, “On the co-polarized phase difference of rough layered surfaces: Formulae derived from the small perturbation method,” *IEEE Trans. Antennas Propag.*, vol. 59, no. 7, pp. 2607–2618, Jul. 2011.

[23] R. Dusséaux and S. Afifi, “Statistical distributions of the co-polarized and cross-polarized phase differences of stratified media,” *IEEE Trans. Antennas Propag.*, vol. 65, no. 3, pp. 1517–1521, Mar. 2017.

[24] S. Afifi and R. Dusséaux, “On the co-polarized scattered intensity ratio of rough layered surfaces: The probability law derived from the small perturbation method,” *IEEE Trans. Antennas Propag.*, vol. 60, no. 4, pp. 2133–2138, Apr. 2012.

[25] S. Afifi and R. Dusséaux, “The co- and cross-polarized scattered intensity ratios for 3D layered structures with randomly rough interfaces,” *J. Electromagn. Waves Appl.*, vol. 33, no. 7, pp. 811–826, 2019.

[26] J.A. Kong, A.A. Swartz, H.A. Yueh, L.M. Novak, and R.T. Shin, “Identification of terrain cover using the optimum polarimetric classifier,” *J. Electromagn. Waves Appl.*, vol. 2, no. 2, pp.171-194,1988.

[27] J.S. Lee, K.W. Hoppel, S. A. Mango, and A. R. Miller, “Intensity and phase statistics of multilook polarimetric and interferometric SAR imagery”, *IEEE Trans. Geosci. Remote Sens.*, vol. 32, no. 5, pp.

1017-1028, Sep. 1994.

[28] I. R. Joughin, D. P. Winebrenner, and D. B. Percival, "Probability density functions for multilook polarimetric signatures," *IEEE Trans. Geosci. Remote Sens.*, vol. 32, no. 3, pp. 562–574, May 1994.

[29] J.-S. Lee and E. Pottier, *Polarimetric Radar Imaging: From Basics to Applications*. Boca Raton, FL, USA: CRC Press, 2009.

[30] R. Dusséaux and S. Afifi, "Multilook intensity ratio distribution for 3-D layered structures with slightly rough interfaces," *IEEE Trans. Antennas Propag.*, vol. 68, no. 7, pp. 5575 – 5582, Jul. 2020.

[31] S. Afifi and R. Dusséaux, "Multilook phase difference distribution for slightly rough boundary layered ground," *IET Microw. Antennas Propag.*, vol.15, no. 7, pp.718-727, Jun. 2021.

[32] R. Barakat, "Statistics of the Stokes parameters," *J. Opt. Soc. Am. A*, vol. 4, no. 7, pp. 1256-1263, Jul. 1987.

[33] R. Touzi and A. Lopes, "Statistics of the Stokes parameters and of the complex coherence parameters in one-look and multilook speckle fields," *IEEE Trans. Geosci. Remote Sens.*, vol. 34, no. 2, pp. 519–531, Mar. 1996.

[34] D. Eliyahu, "Vector statistics of correlated Gaussian fields," *Phys. Rev. E*, vol. 47, no. 4, pp. 2881-2892, Apr. 1993.

[35] K.S. Chen, L. Tsang, K.L. Chen, T. H. Liao, and J-S. Lee, "Polarimetric simulations of SAR at L-band over bare soil using scattering matrices of random rough surfaces from numerical three-dimensional solutions of Maxwell equations," *IEEE Trans. Geosci. Remote Sens.*, vol. 52, no. 11, pp. 7048–7058, Nov. 2014.

[36] R. Gardashov, G. Kara, and E. G. Emecen Kara, "Calculation of the statistical characteristics of the light reflected by a rough random cylindrical homogeneous Gaussian surface," *J. Modern Opt.*, vol. 65, no. 17, pp. 2025-2033, Jun. 2018.

[37] M. Born and E. Wolf, *Principles of optics: Electromagnetic theory of propagation, interference and diffraction of light*. Oxford, U.K.: Pergamon, 1980, appendix III.

[38] C. Baudier and R. Dusséaux, "Scattering of an E// polarized plane wave by one-dimensional rough surfaces: Numerical applicability domain of a Rayleigh method in the far-field zone," *Prog. Electromagn. Res.*, vol. 34, pp. 1–27, 2001.

- [39] A. Ishimaru, *Electromagnetic wave propagation, radiation and scattering*. Englewood Cliffs, NJ: Prentice-Hall, 1991, pp. 298–302.
- [40] J. J. Gil and E. Bernabeu, “A depolarization criterion in Mueller matrices,” *Opt. Acta*, vol. 3, no. 3, pp. 259-261, 1985.
- [41] G. N. Watson, *A Treatise on the Theory of Bessel Functions*. U.K., Cambridge: Cambridge Univ. Press, 1922.
- [42] Y-Q Jin and N-X Zhang, “Statistics of four Stokes parameters in multi-look polarimetric synthetic aperture radar (SAR) imagery,” *Can. J. Remote Sens.*, vol. 28, no. 4, pp 610-619, 2002.